TLR Agonists Delivered by Plant Virus and Bacteriophage Nanoparticles for Cancer Immunotherapy

Eunkyeong Jung,
Department of NanoEngineering, University of California, San Diego, La Jolla, California 92093, United States

Young Hun Chung,
Department of Bioengineering and Moores Cancer Center, University of California San Diego, La Jolla, California 92093, United States

Nicole F. Steinmetz
Department of NanoEngineering, University of California, San Diego, La Jolla, California 92093, United States

Department of Bioengineering, Moores Cancer Center, Center for Nano-ImmunoEngineering, Department of Radiology, and Institute for Materials Discovery and Design, University of California San Diego, La Jolla, California 92093, United States

Abstract

Toll-like receptors (TLRs) are promising targets in cancer immunotherapy due to their role in activating the immune system; therefore, various small-molecule TLR agonists have been tested in clinical applications. However, the clinical use of TLR agonists is hindered by their non-specific side effects and poor pharmacokinetics. To overcome these limitations, we used plant virus nanoparticles (VNPs) and bacteriophage virus-like particles (VLPs) as drug delivery systems. We conjugated TLR3 or TLR7 agonists to cowpea mosaic virus (CPMV) VNPs, cowpea chlorotic mottle virus (CCMV) VNPs, and bacteriophage Qβ VLPs. The conjugation of TLR7 agonist, 2-methoxyethoxy-8-oxo-9-(4-carboxybenzyl)adenine (1V209), resulted in the potent activation of immune cells and promoted the production of pro-inflammatory cytokine interleukin 6. We found that 1V209 conjugated to CPMV, CCMV, and Qβ reduced tumor growth in vivo and prolonged the survival of mice compared to those treated with free 1V209 or a simple admixture of 1V209

Corresponding Author: Nicole F. Steinmetz – Department of NanoEngineering, University of California, San Diego, La Jolla, California 92093, United States; Department of Bioengineering, Moores Cancer Center, Center for Nano-ImmunoEngineering, Department of Radiology, and Institute for Materials Discovery and Design, University of California San Diego, La Jolla, California 92093, United States; nsteinmetz@ucsd.edu.

ASSOCIATED CONTENT

Supporting Information

The Supporting Information is available free of charge at https://pubs.acs.org/doi/10.1021/acs.bioconjchem.3c00271.

Characterization of native CPMV, CCMV, and Qβ particles; in vivo therapeutic efficacy of native CPMV, CCMV, and Qβ particles; characterization of Cy5-labeled CPMV, CCMV, and Qβ particles; biodistribution of Cy5-labeled CPMV, CCMV, and Qβ particles; characterization of CPMV-poly(I:C) particles; and evaluation of NF-κB/AP-1 activation in RAW-Blue cells (PDF)

Complete contact information is available at: https://pubs.acs.org/10.1021/acs.bioconjchem.3c00271

and viral particles. Nucleic acid-based TLR3 agonist, polyinosinic acid with polycytidylic acid (poly(I:C)), was also delivered by CPMV VNPs, resulting in enhanced mice survival. All our data suggest that coupling and co-delivery are required to enhance the anti-tumor efficacy of TLR agonists and simple mixing of the VLPs with the agonists does not confer a survival benefit. The delivery of 1V209 or poly(I:C) conjugated to VNPs/VLPs probably enhances their efficacy due to the multivalent presentation, prolongation of tumor residence time, and targeting of the innate immune cells mediated by the VNP/VLP carrier.

Graphical Abstract
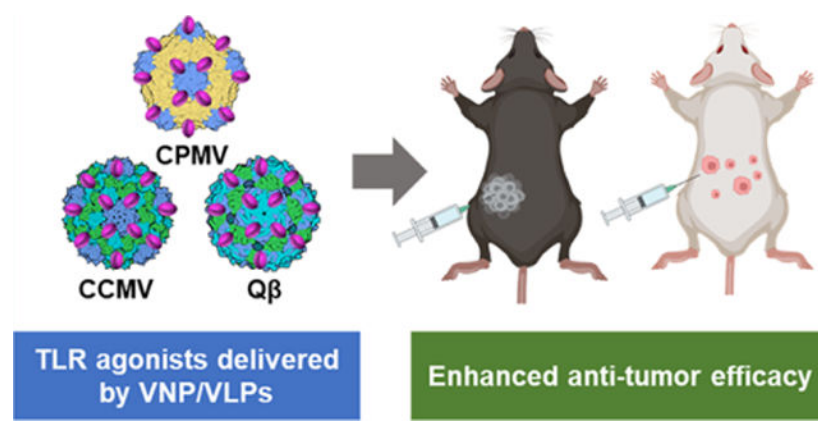
INTRODUCTION

Toll-like receptors (TLRs) are important pattern recognition receptors (PRRs) that are expressed on antigen-presenting cells such as dendritic cells, macrophages, neutrophils, natural killer cells, T cells, and B cells. TLRs detect pathogen-associated molecular patterns (PAMPs) and induce innate immune responses.[1] Following the recognition of PAMPs, TLRs signal through four cytosolic toll-interleukin-1 receptor (TIR) domain-containing adaptor proteins (TIRAPs): myeloid differentiation primary response 88 (MyD88), MyD88 adaptor-like protein (MAL), TIR domain-containing adapter-inducing interferon-β, and TRIF-related adaptor molecule. This results in the activation and translocation of the nuclear factor kappa B transcription factor (NF-κB), interferon (IFN) regulatory factors, and/or mitogen-activated protein kinases (MAPKs) that regulate IFN gene expression.[2] TLR-based immunotherapy has been extensively investigated as either a single or combinational approach because it triggers a strong immune response.[3–5] Accordingly, TLR agonists have been evaluated as promising vaccine adjuvants for cancer treatment.

The TRL7 agonist, 2-methoxyethoxy-8-oxo-9-(4-carboxybenzyl)adenine (1V209), is a synthetic molecule developed as an alternative to imiquimod and the only TRL7 ligand currently approved by the US Food & Drug Administration (FDA).[5,6] Although 1V209 is well known for its anti-tumor effects and immunogenicity, its clinical application is limited by its low solubility and stability and potent cytokine production following systemic administration, resulting in toxicity and hyper-inflammation.[7] The TLR3 agonist, polyinosinic acid with polycytidylic acid (poly(I:C)), is a double-stranded RNA recognized

by endosomal TLR3, which subsequently regulates melanoma differentiation-associated protein 5 (MDA5) and retinoic acid-inducible gene-I protein (RIG-I), ultimately triggering IFN signaling.[8] Poly(I:C) has been investigated as a potent immunostimulant or adjuvant to cancer treatment. Despite the potential efficacy of the nucleic acid derivatives, their applications are limited due to the rapid degradation by nucleases and the toxicity caused by the off-target toxicity.[9] Therefore, various drug delivery platforms have been investigated to overcome the shortcomings of free drug administration and to amplify the therapeutic efficacy using a co-delivery system.

Plant viruses and bacteriophages have emerged as promising drug delivery and immunomodulators. For example, Cowpea mosaic virus (CPMV) is an icosahedral plant virus with a positive-sense bipartite RNA genome and a capsid ~28 nm in diameter. When administered intratumorally (i.t.), CPMV is a potent in situ vaccine that activates TLR2, TLR4, and TRL7, and the resulting anti-tumor immune responses have been investigated in the context of colon cancer, breast cancer, glioma, ovarian cancer, and melanoma.[10–12] CPMV has also been used as a delivery platform for proteins,[13] peptides,[14] small-molecule drugs,[15] and imaging agents[16] through the direct modification of the capsid. Cowpea chlorotic mottle virus (CCMV) is structurally similar to CPMV but has no anti-tumor efficacy.[11] However, it has also been studied as a drug delivery vehicle due to its ability to undergo reversible structural phase transition.[4,17] CCMV can be disassembled and reassembled with cargo by controlling the pH and salt concentrations (Ca^{2+} or Mg^{2+}). We have previously developed a self-assembling CCMV delivery platform for the class B CpG oligodeoxynucleotide ODN1826, which triggers TLR9 signaling. Encapsulated ODN1826 stimulated the tumor-associated macrophages in the tumor microenvironment to a greater extent than did free ODN1826, demonstrating higher efficacy against colon cancer and melanoma.[4] Bacteriophage Qβ is similar in size and structure to the two plant viruses and has been investigated for the delivery of drugs against bacterial infections,[18] cardiovascular diseases,[19] autoimmune disorders,[20] and cancer.[21] CpG-laden Qβ virus-like particles (VLPs) are undergoing clinical testing for cancer therapy.[22]

Here, we developed TLR agonist co-delivery platforms to boost systemic anti-tumor immunity using CPMV, CCMV, and Qβ. TLR agonists have been delivered using various synthetic nanoparticles; here, the issues addressed were, first, whether the addition of TLR agonists would enhance the efficacy of CCMV or Qβ, which alone are not potent immunomodulators when used as an in situ vaccine. Second, whether the addition of the TLR3 agonist could also boost CPMV efficacy because CPMV signals only through TLR2, 4, and 7 but not through TLR3. Third, we probed whether co-delivery is required or whether admixtures could also potentiate efficacy. The anti-tumor efficacy and immunogenicity of 1V209 conjugated to CPMV, CCMV, and Qβ were tested in experimental B16F10 melanoma and CT26 colon cancer models. TLR3 agonist, poly(I:C), was also conjugated to CPMV particles to induce synergy between poly(I:C) and CPMV, which was also tested in the B16F10 melanoma model.

RESULTS AND DISCUSSION

Characterization of 1V209-Conjugated Viral Particles.

We conjugated the TRL7 agonist to plant VNPs and bacteriophage VLPs (Figure 1). We also conjugated the virus particles to poly(I:C) and cyanine 5 (Cy5) for the evaluation of combination therapy and particle stability. CPMV, CCMV, and Qβ were prepared and purified as previously described,[23,24] and the exposed lysine (Lys) residues were reacted with 1V209 using N-hydroxysuccinimide (NHS) and 1-ethyl-3-(3-dimethylaminopropyl)carbodiimide (EDC) chemistry. EDC activates the carboxylic acid group of 1V209, and NHS then forms a stable amine-reactive sulfo-NHS ester that binds the exposed Lys on the viral surfaces. The conjugated particles are hereafter described as CPMV-1V209, CCMV-1V209, and Qβ-1V209.

The conjugation efficiency was determined by subtracting the remaining concentration of free 1V209 after the reaction from the initial 1V209 concentration, revealing that CPMV, CCMV, and Qβ carried 67, 103, and 286 1V209 molecules, respectively. Conjugation was confirmed by agarose gel electrophoresis (Figure 2A). The electrophoretic mobility of CPMV-1V209, CCMV-1V209, and Qβ-1V209 toward the anode increased with the number of conjugated 1V209 molecules (1V209 conjugates to Lys side chains and each conjugation therefore replaces a positive charge). The conjugated particles remained intact, and their morphology was similar to the corresponding native particles, as confirmed by transmission electron microscopy (TEM) (Figures 2B and S1A). Likewise, dynamic light scattering (DLS) experiments showed that the native and conjugated particles had similar average diameters of ~30 nm with no evidence of aggregation (Figure 2C). The size exclusion chromatography (SEC) elution profiles including the absorbance ratios of CPMV-1V209, CCMV-1V209, and Qβ-1V209 at 260/280 nm and the volume of elution were also similar to those of the native particles, further confirming their integrity and purity (Figures 2D and S1B).

Immunogenicity of 1V209-Conjugated Viral Particles.

We investigated the immunogenicity of the 1V209-conjugated VNPs/VLPs using RAW-Blue macrophages, which express various PRRs and a secreted embryonic alkaline phosphatase (SEAP) reporter allowing us to monitor NF-κB activation using a Quanti-Blue assay (Figure 3A). The SEAP level increased sharply in response to CPMV, which was ~5.5-fold higher than CCMV and ~7.4-fold higher than Qβ. This is consistent with prior work that indicates that CPMV is more immunogenic than the other particles due to its multi-pronged ability to trigger TLR2, TLR4, and TLR7 signaling.[11] The admixture of CPMV + 1V209 produced ~1.3-fold more SEAP than CPMV alone, but the admixtures of the other particles with 1V209 did not significantly increase the SEAP activity compared to that in the native particles. In contrast, CPMV-1V209, CCMV-1V209, and Qβ-1V209 increased SEAP activity by ~1.1-fold, ~3.2-fold, and ~4.2-fold, respectively, compared to those by the admixtures of each native particle + 1V209.

Next, we compared the effect of 1V209-conjugated particles on TLR7-mediated interleukin (IL)-6 secretion (Figure 3B). IL-6 levels induced by native CPMV were ~21-fold higher

compared to native CCMV and ~32-fold higher compared to native Qβ, which was consistent with the RAW-Blue assay. The admixtures of CPMV, CCMV, and Qβ with 1V209 activated RAW 264.7 cells at a similar level to each native particle, indicating no synergistic effects with 1V209. In contrast, CPMV-1V209, CCMV-1V209, and Qβ-1V209 significantly increased the IL-6 levels in RAW264.7 cells by ~1.2-fold, ~1.7-fold, and ~7.4-fold, respectively, compared to that in the corresponding admixture groups (Figure 3B). Together, these data indicate that 1V209 must be conjugated to and not co-delivered with the viral particles in order to achieve enhanced immunogenicity.

Therapeutic Efficacy of 1V209-Conjugated Virus Particles In Vivo.

The therapeutic efficacy of the 1V209-conjugated particles was evaluated in dermal melanoma and colon cancer models. For the dermal melanoma model, female C57BL/6 mice were inoculated with B16F10 cells [2×10^5 cells, intradermally (i.d.)]. The particles were injected intratumorally (i.t.) when the tumor reached a volume of ~30 mm^3 (~ day 12) for a total of three weekly injections (Figure 4A). In the mice injected with native CPMV, tumor growth was reduced by 66.5% on day 28 compared to that in the PBS control group (Figure 4B,C). CPMV performed better than CCMV (17.3% growth reduction) and Qβ (22.75% growth reduction) (Figure S2A), which is consistent with the unique anti-cancer immunity induced by CPMV, as previously reported.[11] The admixture of CPMV + 1V209 inhibited tumor growth by 68%, which was similar to that of CPMV alone. However, CPMV-1V209 inhibited tumor growth by 85% (Figure 4B,C) and increased the median survival rate to 50 days (Figure 4D), which was an improvement compared to the other groups (PBS control, 26 days; CPMV, 33 days; and CPMV + 1V209, 35 days). CCMV and the admixture of CCMV + 1V209 inhibited tumor growth on day 28 by 17.2 and 26.8%, respectively (Figure 4B,C), and resulted in median survival rates of 24 and 30 days, respectively, indicating no significant anti-tumor efficacy. However, CCMV-1V209 inhibited tumor growth by 54.6% on day 28 and prolonged the median survival period to 33 days (Figure 4D). Similarly, Qβ and the admixture of Qβ + 1V209 inhibited tumor growth on day 28 by 22.7 and 10%, respectively (Figure 4B,C), and the median survival periods were 27 and 28 days, respectively (Figure 4D). However, Qβ-1V209 showed a potent anti-cancer effect, inhibiting tumor growth by 80% and prolonging the median survival period to 33 days. When comparing CCMV and Qβ, neither particle was efficacious as a solo therapy, but Qβ-1V209 performed better than CCMV-1V209 presumably because more 1V209 molecules were conjugated to each Qβ particle (Figure 1).

In the CT26 colon cancer model, BALB/c mice were challenged intraperitoneally (i.p.) with CT26 cells and treated with particles 3 days post-inoculation (Figure 5A). CPMV inhibited tumor growth by 26.5% compared to that in the PBS-treated controls on day 22 and was significantly more effective than CCMV and Qβ (Figure S2B). The admixture of CPMV + 1V209 and the CPMV-1V209 particles did not show any synergistic inhibition of tumor growth compared to native CPMV, with 24.6 and 28.5% inhibition on day 22, respectively (Figure 5B,C). The median survival periods for the native CPMV, admixture, and conjugated particles were 30, 30, and 34 days, respectively (Figure 5D). The similar performance of the three CPMV-based treatments probably reflects the already potent anti-tumor effect of native CPMV in the CT26 colon cancer model.[11] CCMV and the admixture of CCMV +

1V209 inhibited tumor growth by 8.4 and 6.5% on day 22, respectively, which did not differ significantly from the PBS control (Figure 5B,C). Similarly, the median survival periods of the PBS control, CCMV, and CCMV + 1V209 admixture were 22, 20, and 22 days, respectively (Figure 5D), confirming that these formulations showed no anti-tumor efficacy. However, CCMV-1V209 reduced tumor growth by 17.5% compared to the PBS control on day 22 and prolonged the survival to 30 days. Finally, Qβ-1V209 reduced tumor growth by 21% compared to the PBS control, whereas the native Qβ particles (0.65% reduction) and admixture with 1V209 (12.2% reduction) did not show a significant effect. CCMV-1V209 was less effective than Qβ-1V209, again presumably due to the number of conjugated drug molecules. The accumulation of blood and other body fluids in the peritoneal space increased the circumference and body weight of the treated mice (Figure 5B,E).

We also assessed the retention of CPMV, CCMV, and Qβ in tumors after intratumoral administration to understand the relationship between particle stability and therapeutic efficacy. Long-term tumor retention and multivalent/polyvalent binding of TLRs are important factors for in situ vaccination, which determine therapeutic efficacy.[25] For live animal IVIS imaging, CPMV, CCMV, and Qβ were labeled with Cy5, resulting in CPMV-Cy5, CCMV-Cy5, and Qβ-Cy5 particles. These were characterized by agarose gel electrophoresis and SEC to confirm their integrity (Figures S2 and S3) before injection into mice bearing B16F10 tumors with a volume of at least ~100 mm^3. The intratumoral. injection of CPMV-Cy5, CCMV-Cy5, and Qβ-Cy5 resulted in similar retention times exceeding 7 days in all tumors (Figure S4), suggesting that the observed differences in therapeutic efficacy reflect the conjugation efficiency rather than the stability of each type of particle. Future studies should also focus on detailing the biodistribution of the cargo; while 1V209 is a stable molecule, it is a small molecule that may suffer rapid wash-out effects if cleaved from the nanoparticle surface. Also, the poly(I:C) agonist may be prone to degradation, and future studies need to detail whether the nanocarrier confers advantages by reducing nuclease access, thereby increasing the stability of poly(I:C).

Characterization, Immunogenicity, and Efficacy of Poly(I:C)-Conjugated Viral Particles.

We previously demonstrated that CPMV exerts its potent immunogenicity by activating TLR2, TLR4, and TLR7.[10] The combination of CPMV and 1V209 showed moderate improvement compared to native CPMV, which may be explained by the fact that CPMV already signals through TLR7. While the conjugation of 1V209 to CPMV did not increase efficacy, therapeutic effect was more potent for CCMV-1V209 and Qβ-1V209 vs their non-conjugated versions when tested in the B16F10 and CT26 models (Figures 4 and 5). CCMV and Qβ do not signal through TLR7. Therefore, to determine whether synergy could be achieved by combining CPMV with TLRs other than TLR2, TLR4, and TLR7, we combined it with the TLR3 agonist poly(I:C). The amine residues in CPMV were conjugated to poly(I:C) using EDC and 1-methylimidazole (MeIm) (Figure S5A). The 5′-end phosphate group of poly(I:C) was functionalized by EDC and MeIm to form a phosphoramidate in the presence of the primary amine group of CPMV Lys residues. The conjugation efficiency was measured by subtracting the free poly(I:C) remaining after conjugation from the total initial amount, revealing the presence of ~25 poly(I:C) strands per particle. CPMV and the conjugated derivative CPMV-poly(I:C) were shown to be monodisperse, icosahedral

particles by TEM, and DLS indicated particle diameters of ~31.7 nm (PDI = 0.1) and ~34.5 nm (PDI = 0.22), respectively (Figure S5B,C). The surface charge of CPMV was recorded as −13.5 mV, which increased to −5.6 mV following conjugation (Figure S5D). Accordingly, the poly(I:C)-conjugated CPMV were less mobile in agarose gels compared to the native CPMV particles (Figure S5E). The underlying factor that contributes to the lower negative zeta potential is counterintuitive because poly(I:C) carries negative charge; nevertheless, zeta potential and native gels show consistent results. SEC confirmed the structural integrity of CPMV and CPMV-poly(I:C) with the same elution volume of ~11 mL and an absorbance ratio at 260/280 nm of ~1.7, indicating intact capsid proteins and RNAs (Figure S5F).

We next investigated the immunogenicity of CPMV-poly-(I:C) using RAW-Blue cells (Figure S6). Native CPMV and the CPMV + poly(I:C) admixture activated RAW-Blue cells to a similar extent, but the CPMV-poly(I:C) particles increased the amount of SEAP by ~1.3-fold compared to that in CPMV. To investigate the potential synergistic effect of CPMV and poly(I:C) in vivo, B16F10 cells were injected i.d. into the flank of C57BL/6 mice. When the tumor reached a volume of ~30 mm^3 (~ day 12), we administrated native, admixed or conjugated particles (Figure 6A). CPMV-poly(I:C) did not inhibit tumor growth to a significantly greater extent than the native CPMV particles (Figure 6B) but prolonged the median survival period to 52 days, compared to 33 days for the native particles and 39 days for the CPMV + poly(I:C) admixture (Figure 6C). This data may indicate that the addition of further TLR agonists to CPMV does not confer enhanced anti-tumor potency potentially due to the similar signaling pathways between TLRs. Adding TLR3 does not do much because the maximum signaling through that pathways has already been reached. In other work, we will focus on other combinations, e.g., we already demonstrated synergy with NK agonists,[26] checkpoint inhibitors,[27] radiation therapy,[28] cryoablation,[29] and chemotherapy.[30]

CONCLUSIONS

TLR agonists are powerful adjuvants for cancer immunotherapy. We have demonstrated the potential of a nanoscale TLR agonist, namely small molecule 1V109 or poly(I:C), conjugated to the plant viruses CPMV and CCMV and bacteriophage Qβ to act as immunomodulators for intratumoral immunotherapy. The conjugated, nanoscale TLR7 agonist (CPMV-1V209, CCMV-1V209, and Qβ-1V209) activated immune cells, induced the production of pro-inflammatory cytokines, and inhibited tumor growth in the B16F10 melanoma and CT26 colon cancer models. The CCMV-1V209 and Qβ-1V209 conjugates showed greater therapeutic efficacy than the admixtures of each native particle and 1V209, confirming that drug carriers are necessary to improve drug efficacy. CPMV did not show a significant synergistic effect when combined with TLR3 and TLR7 agonists. This also demonstrates that CPMV itself is a potent immuno-adjuvant that may not benefit from additional TLR activation.

MATERIALS AND METHODS

Preparation of CPMV, CCMV, and Qβ.

CPMV and CCMV were produced in black-eyed pea no. 5 plants as previously described.[24,31] Qβ was expressed in *Escherichia coli* BL21 (D3) cells as previously

reported.[23] All the viral particles were purified by ultracentrifugation in a sucrose gradient. The concentrations of CPMV and CCMV were determined by UV-vis spectroscopy and Beer-Lambert Law using the specific extinction coefficients of 8.1 and 5.85 mg^{-1} mL cm^{-1}, respectively. The concentration of Qβ was verified using a Pierce BCA protein assay kit (Thermo Fisher Scientific).

Bioconjugation of CPMV, CCMV, and Qβ.

CPMV and Qβ were suspended in 10 mM potassium phosphate (KP) buffer (pH 7.0), whereas CCMV was suspended in 10 mM *N*-2-hydroxyethylpiperazine-*N'*-2-ethanesulfonic acid (HEPES) buffer (pH 7.4). 2400 molar excess of free 1V209 (MedChem Express) was activated with NHS and EDC in dimethyl sulfoxide for 2 h before mixing with CPMV, CCMV, and Qβ suspensions and incubating for 2 h at room temperature (RT). The particles were then purified using PD MidiTrap G-25 columns (Cytiva) and 0.5 mL of 100 kDa molecular weight cutoff (MWCO) spin filters (EMD Millipore). The amount of 1V209 conjugated to CPMV, CCMV, and Qβ was calculated by subtracting the concentration of 1V209 remaining in the supernatant from the total added to the reaction (determined by measuring the absorbance at 283 nm). For poly(I:C) conjugation, 2000 molar excess of poly(I:C) (InvivoGen) was activated with EDC and MeIm in nuclease-free water for 30 min at RT before mixing with CPMV and incubating for 2 h at RT. Excess reagent was removed by ultracentrifugation (52,000g, 2 h, 4 °C), and the supernatant was collected to determine the conjugation efficiency. The concentration of poly(I:C) in the supernatant was determined by measuring the absorbance at 266 nm using UV–vis. The amount of poly(I:C) conjugated to the particles was determined by subtracting the unconjugated fraction from the total poly(I:C). For Cy5 labeling reactions, CPMV, CCMV, and Qβ were mixed with 700 molar excess of sulfo-Cy5 NHS ester (Lumiprobe) for 2 h at RT. The reaction mixtures were purified on a 30% (w/v) sucrose cushion by ultracentrifugation (52,000g, 2 h, 4 °C) to remove excess Cy5 dye. The conjugation of Cy5 was quantified based on the dye-to-VNP/VLP ratio and the Beer–Lambert law (molecular weight of CPMV = 5.6×10^6 g mol^{-1}, CCMV = 2×10^4 g mol^{-1}, Qβ = 3.6×10^4 g mol^{-1}, and Cy5 = 747 g mol^{-1}). The number of Cy5 dyes per particle was determined by UV-vis spectroscopy (using a Nanodrop 2000) and Beer-Lambert Law based on the specific extinction coefficients (CPMV$_{\varepsilon260}$ = 8.1 mg^{-1} mL cm^{-1}, CCMV$_{\varepsilon260}$ = 5.85 mg^{-1} mL cm^{-1}, Q$\beta_{\varepsilon260}$ = 8.1 mg^{-1} mL cm^{-1}, and Cy5$_{\varepsilon647}$ = 271,000 mg^{-1} mL cm^{-1}). All native and conjugated CPMV, CCMV, and Qβ particles were stored at 4 °C until needed for further analysis.

Gel Electrophoresis.

CPMV and Qβ particles (10 μg) were analyzed by 0.8% (w/v) agarose native gel electrophoresis in Tris–acetate–EDTA buffer for 30 min at 120 V and RT. CCMV particles were analyzed using the same method but in virus electrophoresis buffer (0.1 M sodium acetate, 1 mM EDTA, pH 5.5) for 60 min at 60 V and 4 °C as previously described.[17] Agarose gels were stained with GelRed nucleic acid to detect RNA and Coomassie brilliant blue to detect protein. The gels were imaged using an AlphaImager System under UV light, white light, and MultiFluor red light for visualization of RNA, protein, and Cy5, respectively.

Transmission Electron Microscopy.

CPMV, CCMV, and Qβ particles were suspended at 1 mg mL^{-1} in deionized water and deposited onto Formvar carbon film-coated copper TEM grids (Ted Pella) for 2 min, followed by washing twice with deionized water for 1 min. The TEM grids were coated with 2% (w/v) uranyl acetate for 2 min. TEM images were acquired using a JEOL JEM-1400Plus microscope.

Dynamic Light Scattering.

CPMV, CCMV, and Qβ particles were dispersed at a concentration of 0.1 mg mL^{-1} in 0.1 M KP buffer for CPMV and Qβ and 0.1 M sodium acetate buffer (pH 4.8) for CCMV. The size was measured on a Zetasizer Nano ZSP/Zen5600 (Malvern Panalytical).

Size Exclusion Chromatography.

CPMV, CCMV, and Qβ particles were prepared at a concentration of 3 mg mL^{-1} and loaded onto a Superose 6 Increase column mounted on an ÄKTA pure chromatography system (Cytiva). The flow rate was set to 0.5 mL min^{-1} in 0.1 M KP buffer for CPMV and Qβ or 0.1 M sodium acetate buffer for CCMV. The absorbance was recorded at 260 and 280 nm, and the fluorescent particles were also measured at 647 nm to detect Cy5.

Cell Studies.

B16F10 (ATCC CRL-6475, mouse skin melanoma) and CT26 (ATCC, mouse colon cancer) cells were cultured in Dulbecco's modified Eagle's medium (DMEM) and Roswell Park Memorial Institute (RPMI) 1640 medium, respectively, each supplemented with 10% (v/v) fetal bovine serum (FBS; Atlanta Biologicals) and 1% (v/v) penicillin/streptomycin (P/S; Thermo Fisher Scientific). RAW-Blue cells (InvivoGen) were grown in DMEM supplemented with 10% (v/v) FBS, 1% (v/v) P/S, 50 mg mL^{-1} normocin, and 100 mg mL^{-1} zeocin and were maintained according to the supplier's instructions. RAW264.7 (ATCC) macrophages were grown in DMEM supplemented with 10% (v/v) FBS and 1% (w/v) P/S. All cells were maintained at 37 °C in a humidified incubator with a 5% CO_2 atmosphere.

RAW-Blue Assay.

RAW-Blue cells were seeded in 96-well plates (1 × 10^5 cells/well) and treated with 1 μg of native or 1V209-conjugated CPMV, CCMV, and Qβ (as well as controls). After 24 h, 20 μL of the supernatant from each well was mixed with 180 μL of Quanti-Blue solution (InvivoGen) and incubated for 6 h at RT before recording the absorbance at 630 nm on a Tecan plate reader.

Enzyme-Linked Immunosorbent Assay.

RAW264.7 cells were seeded into 24-well plates (5 × 10^5 cells/well) and treated with 5 μg of native or 1V209-conjugated CPMV, CCMV, and Qβ. After 24 h, the supernatants were collected from each well and the quantities of IL-6 were determined using the appropriate enzyme-linked immunosorbent assay (ELISA) kits (Thermo Fisher Scientific).

Animal Studies.

C57BL/6 and BALB/c mice (The Jackson Laboratory) were used for animal experiments carried out in accordance with the guidelines set out by the Institutional Animal Care and Use Committee of the University of California, San Diego. For the melanoma model, C57BL/6 mice were inoculated i.d. with B16F10 cells (2×10^5 cells in 20 μL of PBS) in the left flank. The mice then i.t. received three treatments with native or conjugated CPMV, CCMV, and Qβ particles starting 12 days post-inoculation with 1 week intervals between injections. Animal survival and tumor volume were recorded every 2 days, and the tumor volume was calculated using the following equation: tumor volume = (tumor width^2 × tumor length)/2. For the colon cancer model, BALB/c mice were injected i.p. with CT26 cells (5×10^5 cells in 100 μL of PBS). The mice then i.p. received three treatments with native or conjugated CPMV, CCMV, and Qβ particles starting on day 3 with 1 week intervals between the injections. We measured the change in the abdominal circumference with a measuring tape and monitored the body weight of the mice every 2 days.

Fluorescence Imaging.

Mice were inoculated i.d. with B16F10 cells (2×10^5 cells in 20 μL of PBS). When the tumors had grown to ~100 mm^3, Cy5-conjugated CPMV, CCMV, and Qβ particles (100 μg in 20 μL of PBS) were injected into the tumors. Fluorescent images were acquired using an in vivo imaging system (IVIS, Xenogen), and longitudinal imaging was carried out for 7 days.

Statistical Analysis.

Data from in vitro and in vivo studies were analyzed in GraphPad Prism v8 and are presented as means ± standard deviations. For multiple comparisons, statistical significance was determined using one-way ANOVA with a post-hoc Tukey's HSD test. For survival data, curves were generated according to the Mantel–Cox test and were compared statistically using the log-rank test. Significance was assigned at $P < 0.05$.

Supplementary Material

Refer to Web version on PubMed Central for supplementary material.

ACKNOWLEDGMENTS

REFERENCES

(1). Kawai T; Akira S The role of pattern-recognition receptors in innate immunity: update on Toll-like receptors. Nat. Immunol. 2010, 11, 373–384. [PubMed: 20404851]

(2). O'Neill LA; Bowie AG The family of five: TIR-domain-containing adaptors in Toll-like receptor signalling. Nat. Rev. Immunol. 2007, 7, 353–364. [PubMed: 17457343]

(3). Dongye Z; Li J; Wu Y Toll-like receptor 9 agonists and combination therapies: strategies to modulate the tumour immune microenvironment for systemic anti-tumour immunity. Br. J. Cancer 2022, 127, 1584–1594. [PubMed: 35902641]

(4). Cai H; Shukla S; Steinmetz NF The Antitumor Efficacy of CpG Oligonucleotides is Improved by Encapsulation in Plant Virus-Like Particles. Adv. Funct. Mater. 2020, 30, 1908743. [PubMed: 34366757]

(5). Nkanga CI; Ortega-Rivera OA; Steinmetz NF Photothermal immunotherapy of melanoma using TLR-7 agonist laden tobacco mosaic virus with polydopamine coat. Nanomedicine 2022, 44, 102573. [PubMed: 35728739]

(6). Chan M; Hayashi T; Mathewson RD; Yao S; Gray C; Tawatao RI; Kalenian K; Zhang Y; Hayashi Y; Lao FS; et al. Synthesis and characterization of PEGylated toll like receptor 7 ligands. Bioconjugate Chem. 2011, 22, 445–454.

(7). (a)Shinchi H; Crain B; Yao S; Chan M; Zhang SS; Ahmadiiveli A; Suda Y; Hayashi T; Cottam HB; Carson DA Enhancement of the Immunostimulatory Activity of a TLR7 Ligand by Conjugation to Polysaccharides. Bioconjugate Chem. 2015, 26, 1713–1723.(b)Wan D; Que H; Chen L; Lan T; Hong W; He C; Yang J; Wei Y; Wei X Lymph-Node-Targeted Cholesterolized TLR7 Agonist Liposomes Provoke a Safe and Durable Antitumor Response. Nano Lett. 2021, 21, 7960–7969. [PubMed: 34533963]

(8). (a)Slater L; Bartlett NW; Haas JJ; Zhu J; Message SD; Walton RP; Sykes A; Dahdaleh S; Clarke DL; Belvisi MG; et al. Co-ordinated role of TLR3, RIG-I and MDA5 in the innate response to rhinovirus in bronchial epithelium. PLoS Pathog. 2010, 6, No. e1001178. [PubMed: 21079690] (b)Yu M; Levine SJ Toll-like receptor 3, RIG-I-like receptors and the NLRP3 inflammasome: Key modulators of innate immune responses to double-stranded RNA viruses. Cytokine Growth Factor Rev. 2011, 22, 63–72. [PubMed: 21466970]

(9). Longhi MP; Trumpfheller C; Idoyaga J; Caskey M; Matos I; Kluger C; Salazar AM; Colonna M; Steinman RM Dendritic cells require a systemic type I interferon response to mature and induce CD4+ Th1 immunity with poly IC as adjuvant. J. Exp. Med. 2009, 206, 1589–1602. [PubMed: 19564349]

(10). Mao C; Beiss V; Fields J; Steinmetz NF; Fiering S Cowpea mosaic virus stimulates antitumor immunity through recognition by multiple MYD88-dependent toll-like receptors. Biomaterials 2021, 275, 120914. [PubMed: 34126409]

(11). Shukla S; Wang C; Beiss V; Cai H; Washington T 2nd; Murray AA; Gong X; Zhao Z; Masarapu H; Zlotnick A; et al. The unique potency of Cowpea mosaic virus (CPMV) in situ cancer vaccine. Biomater. Sci. 2020, 8, 5489–5503. [PubMed: 32914796]

(12). (a)Shukla S; Myers JT; Woods SE; Gong X; Czapar AE; Commandeur U; Huang AY; Levine AD; Steinmetz NF Plant viral nanoparticles-based HER2 vaccine: Immune response influenced by differential transport, localization and cellular interactions of particulate carriers. Biomaterials 2017, 121, 15–27. [PubMed: 28063980] (b)Lizotte PH; Wen AM; Sheen MR; Fields J; Rojanasopondist P; Steinmetz NF; Fiering S In situ vaccination with cowpea mosaic virus nanoparticles suppresses metastatic cancer. Nat. Nanotechnol. 2016, 11, 295–303. [PubMed: 26689376]

(13). Chung YH; Park J; Cai H; Steinmetz NF S100A9-Targeted Cowpea Mosaic Virus as a Prophylactic and Therapeutic Immunotherapy against Metastatic Breast Cancer and Melanoma. Adv. Sci. 2021, 8, No. e2101796.

(14). Gautam A; Beiss V; Wang C; Wang L; Steinmetz NF Plant Viral Nanoparticle Conjugated with Anti-PD-1 Peptide for Ovarian Cancer Immunotherapy. Int. J. Mol. Sci. 2021, 22, 9733. [PubMed: 34575893]

(15). Aljabali AA; Shukla S; Lomonossoff GP; Steinmetz NF; Evans DJ CPMV-DOX delivers. Mol. Pharm. 2013, 10, 3–10. [PubMed: 22827473]

(16). Affonso de Oliveira JF; Chan SK; Omole AO; Agrawal V; Steinmetz NF In Vivo Fate of Cowpea Mosaic Virus In Situ Vaccine: Biodistribution and Clearance. ACS Nano 2022, 16, 18315–18328. [PubMed: 36264973]

(17). Chan SK; Du P; Ignacio C; Mehta S; Newton IG; Steinmetz NF Biomimetic Virus-Like Particles as Severe Acute Respiratory Syndrome Coronavirus 2 Diagnostic Tools. ACS Nano 2021, 15, 1259–1272. [PubMed: 33237727]

(18). Crooke SN; Schimer J; Raji I; Wu B; Oyelere AK; Finn MG Lung Tissue Delivery of Virus-Like Particles Mediated by Macrolide Antibiotics. Mol. Pharm. 2019, 16, 2947–2955. [PubMed: 31244221]

(19). Crossey E; Amar MJA; Sampson M; Peabody J; Schiller JT; Chackerian B; Remaley AT A cholesterol-lowering VLP vaccine that targets PCSK9. Vaccine 2015, 33, 5747–5755. [PubMed: 26413878]

(20). Rohn TA; Jennings GT; Hernandez M; Grest P; Beck M; Zou Y; Kopf M; Bachmann MF Vaccination against IL-17 suppresses autoimmune arthritis and encephalomyelitis. Eur. J. Immunol. 2006, 36, 2857–2867. [PubMed: 17048275]

(21). (a)Mohsen MO; Vogel M; Riether C; Muller J; Salatino S; Ternette N; Gomes AC; Cabral-Miranda G; El-Turabi A; Ruedl C; et al. Targeting Mutated Plus Germline Epitopes Confers Preclinical Efficacy of an Instantly Formulated Cancer Nano-Vaccine. Front. Immunol. 2019, 10, 1015. [PubMed: 31156619] (b)Wu X; Yin Z; McKay C; Pett C; Yu J; Schorlemer M; Gohl T; Sungsuwan S; Ramadan S; Baniel C; et al. Protective Epitope Discovery and Design of MUC1-based Vaccine for Effective Tumor Protections in Immunotolerant Mice. J. Am. Chem. Soc. 2018, 140, 16596–16609. [PubMed: 30398345] (c)Wu X; McKay C; Pett C; Yu J; Schorlemer M; Ramadan S; Lang S; Behren S; Westerlind U; Finn MG; et al. Synthesis and Immunological Evaluation of Disaccharide Bearing MUC-1 Glycopeptide Conjugates with Virus-like Particles. ACS Chem. Biol. 2019, 14, 2176–2184. [PubMed: 31498587]

(22). Cheng Y; Lemke-Miltner CD; Wongpattaraworakul W; Wang Z; Chan CHF; Salem AK; Weiner GJ; Simons AL In situ immunization of a TLR9 agonist virus-like particle enhances anti-PD1 therapy. J. Immunother. Cancer. 2020, 8, No. e000940. [PubMed: 33060147]

(23). Ortega-Rivera OA; Pokorski JK; Steinmetz NF A single-dose, implant-based, trivalent virus-like particle vaccine against "cholesterol checkpoint" proteins. Adv. Ther. 2021, 4, 2100014.

(24). Leong HS; Steinmetz NF; Ablack A; Destito G; Zijlstra A; Stuhlmann H; Manchester M; Lewis JD Intravital imaging of embryonic and tumor neovasculature using viral nanoparticles. Nat. Protoc. 2010, 5, 1406–1417. [PubMed: 20671724]

(25). (a)Momin N; Palmeri JR; Lutz EA; Jailkhani N; Mak H; Tabet A; Chinn MM; Kang BH; Spanoudaki V; Hynes RO; et al. Maximizing response to intratumoral immunotherapy in mice by tuning local retention. Nat. Commun. 2022, 13, 109. [PubMed: 35013154] (b)Jeganathan S; Budziszewski E; Hernandez C; Dhingra A; Exner AA Improving Treatment Efficacy of In Situ Forming Implants via Concurrent Delivery of Chemotherapeutic and Chemosensitizer. Sci. Rep. 2020, 10, 6587. [PubMed: 32313056]

(26). Koellhoffer EC; Steinmetz NF Cowpea Mosaic Virus and Natural Killer Cell Agonism for In Situ Cancer Vaccination. Nano Lett. 2022, 22, 5348–5356. [PubMed: 35713326]

(27). Wang C; Steinmetz NF A Combination of Cowpea Mosaic Virus and Immune Checkpoint Therapy Synergistically Improves Therapeutic Efficacy in Three Tumor Models. Adv. Funct. Mater. 2020, 30, 2002299. [PubMed: 34366758]

(28). Hoopes PJ; Wagner RJ; Duval K; Kang K; Gladstone DJ; Moodie KL; Crary-Burney M; Ariaspulido H; Veliz FA; Steinmetz NF; et al. Treatment of Canine Oral Melanoma with Nanotechnology-Based Immunotherapy and Radiation. Mol. Pharm. 2018, 15, 3717–3722. [PubMed: 29613803]

(29). Ghani MA; Bangar A; Yang Y; Jung E; Sauceda C; Mandt T; Shukla S; Webster NJG; Steinmetz NF; Newton IG Treatment of Hepatocellular Carcinoma by Multimodal In Situ Vaccination Using Cryoablation and a Plant Virus Immunostimulant. J. Vasc. Intervent. Radiol. 2023, 34, 1247–1257.e8.

(30). Cai H; Wang C; Shukla S; Steinmetz NF Cowpea Mosaic Virus Immunotherapy Combined with Cyclophosphamide Reduces Breast Cancer Tumor Burden and Inhibits Lung Metastasis. Adv. Sci. 2019, 6, 1802281.

(31). (a)Ali A; Roossinck MJ Rapid and efficient purification of Cowpea chlorotic mottle virus by sucrose cushion ultracentrifugation. J. Virol. Methods 2007, 141, 84–86. [PubMed: 17188758] (b)Wen AM; Lee KL; Yildiz I; Bruckman MA; Shukla S; Steinmetz NF Viral Nanoparticles for *In vivo* Tumor Imaging. J. Visualized Exp. 2012, No. e4352.
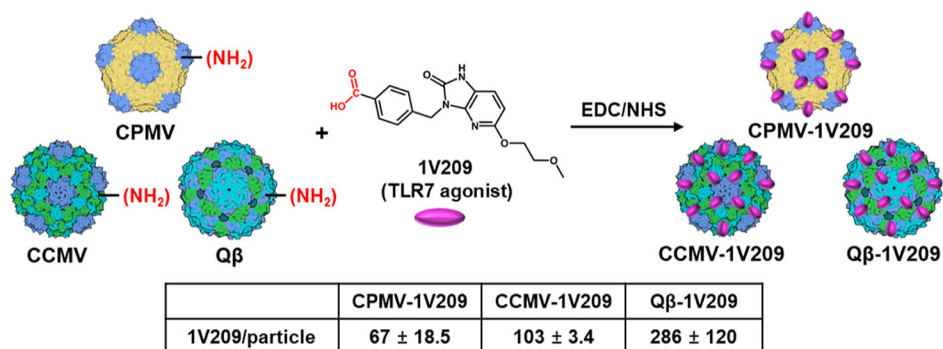
Figure 1.
Synthesis of CPMV-1V209, CCMV-1V209, and Qβ-1V209 particles. We used EDC/NHS chemistry, and the resulting conjugation efficiency was determined by UV–vis absorbance spectrophotometry. Data are mean ± standard deviation ($n = 3$). EDC—1-ethyl-3-(3-dimethylaminopropyl)carbodiimide, NHS—N-hydroxysuccinimide.
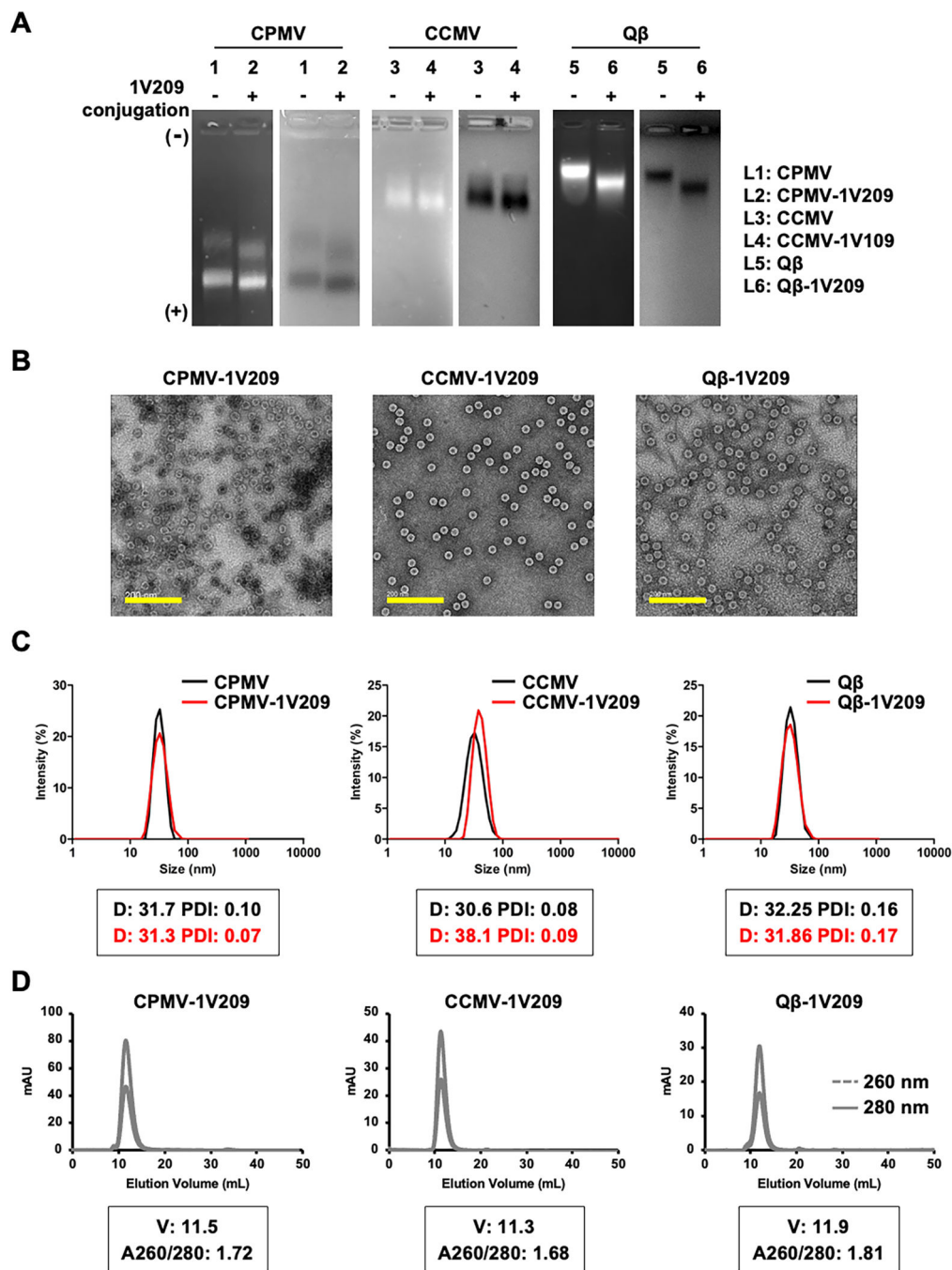
Figure 2.

Characterization of CPMV-1V209, CCMV-1V209, and Qβ-1V209 particles. (A) Analysis of 1V209-conjugated and native particles by 0.8% (w/v) agarose gel electrophoresis. Gels were stained with GelRed and visualized under UV light (left panel, RNA detection) and stained with Coomassie brilliant blue and visualized under white light (right panel, protein detection). The conjugation drives the migration from the cathode (−, top) toward the anode (+, bottom). (B) Representative TEM images (scale bar = 200 nm). (C) Size distribution of the particles determined by DLS. The boxed insets show the average diameter (*D*, nm)

and polydispersity (PDI) of the particles. (D) SEC profiles of the conjugated particles. The boxed insets show the elution volume (V, mL) and the absorbance ratio at 260 and 280 nm (A260/280).
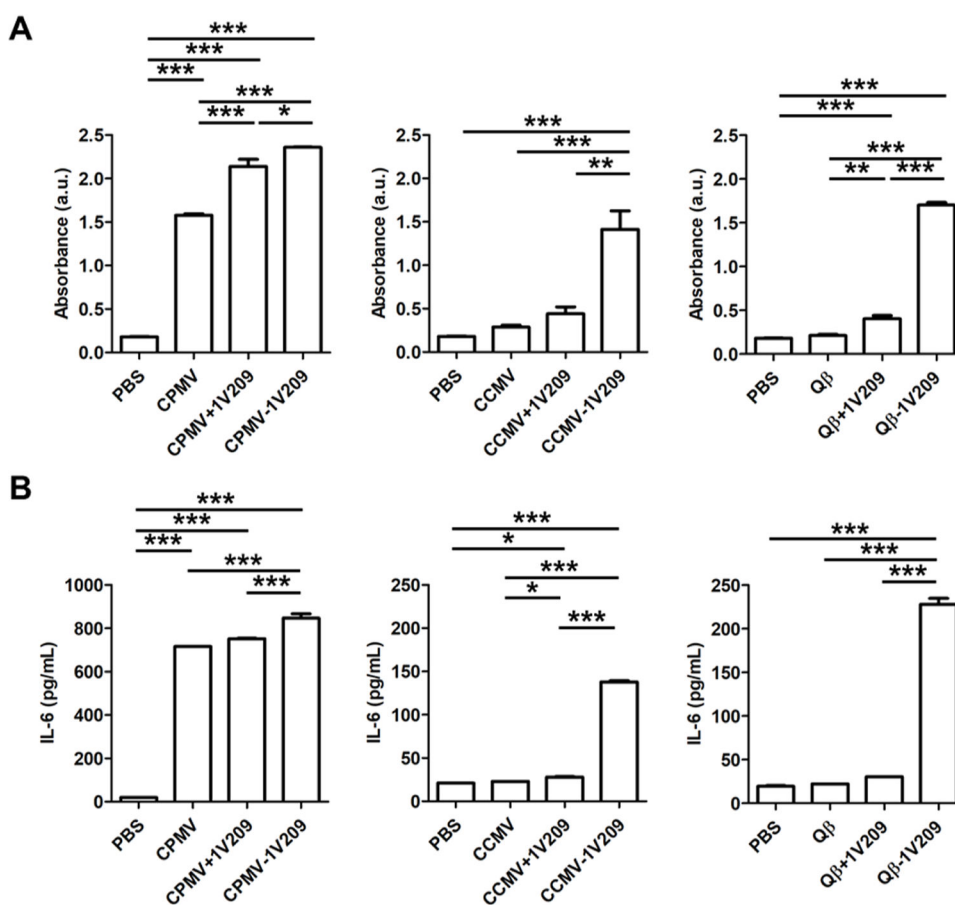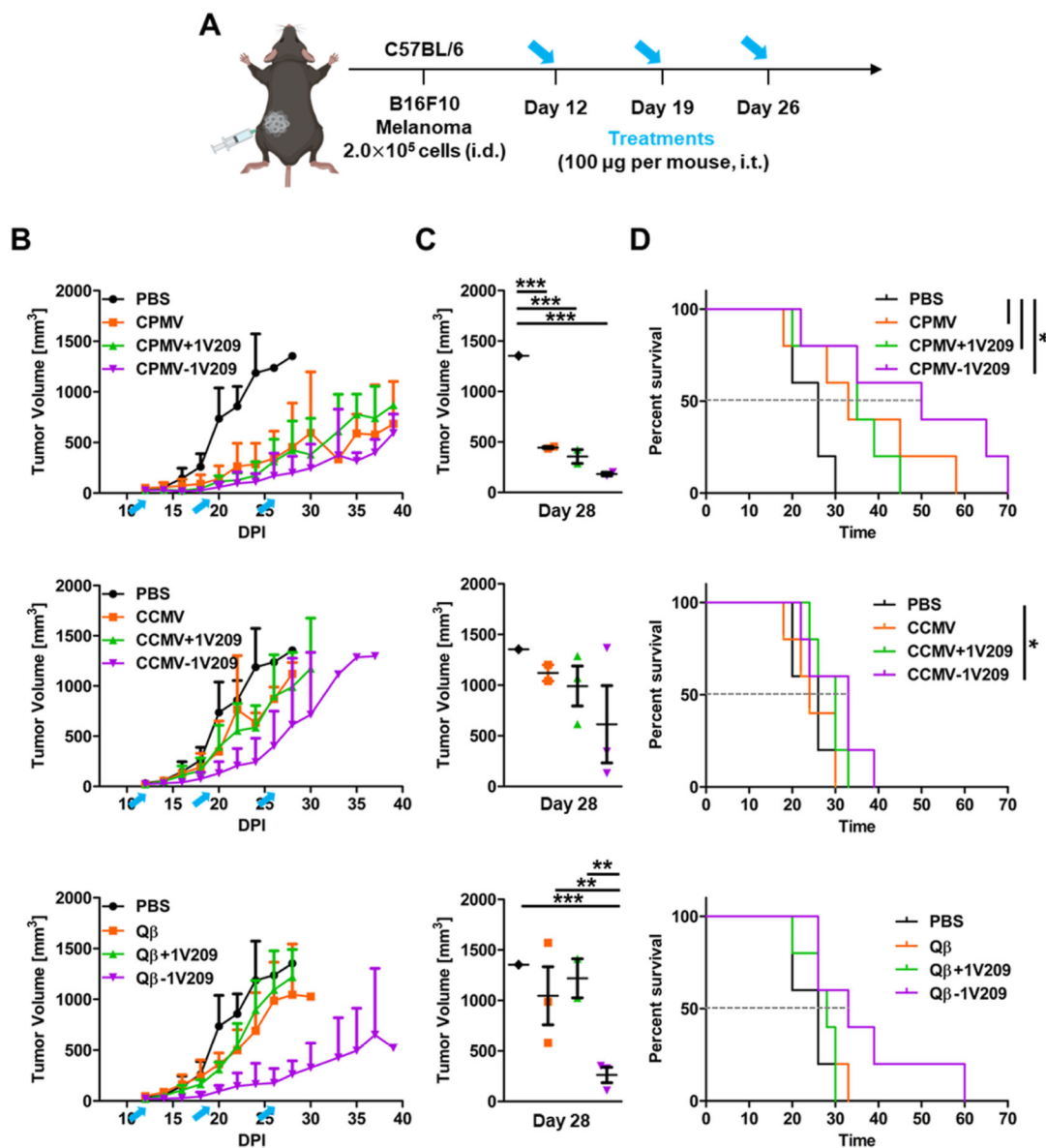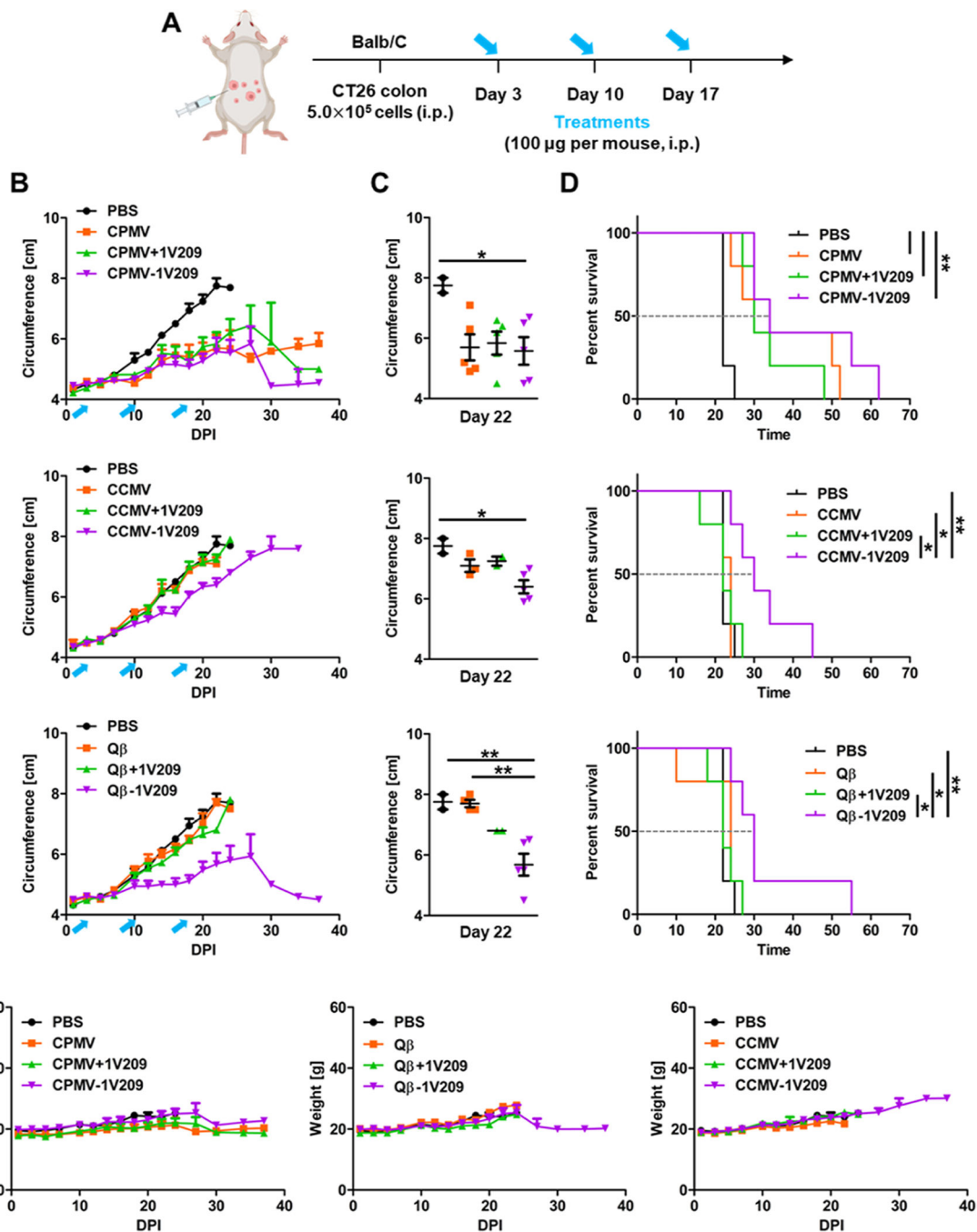
Figure 3.
The immunogenicity of 1V209 is enhanced by conjugation to CPMV, CCMV, and Qβ. (A) Evaluation of NF-κB/AP-1 activation in RAW-Blue cells. (B) IL-6 levels measured by ELISA. The admixture of VNPs/VLPs and 1V209 is named as VNPs/VLPs + 1V209, and the conjugation of VNPs/VLPs and 1V209 is named as VNPs/VLPs − 1V209. Data are means ± SEM ($n = 6$). The results were compared by one-way ANOVA with Tukey's multiple comparisons test (***$P < 0.001$, **$P < 0.01$, and *$P < 0.05$).

Figure 4.

Therapeutic effects of CPMV-1V209, CCMV-1V209, and Qβ-1V209 particles in the in vivo B16F10 melanoma model. (A) Timeline of B16F10 cell inoculation and intratumoral particle injections. (B) Tumor growth curves. Blue arrows indicate the treatment days. (C) Volumetric scatter plot of individual tumors on day 28. Data are means ± SEM ($n = 5$). The results were compared by one-way ANOVA with Tukey's multiple comparisons test (***$P < 0.001$ and **$P < 0.01$). (D) Survival rates of tumor-bearing mice over 70 days (dashed lines show the intersection with median survival for each treatment). The results were compared using the log-rank (Mantel–Cox) test (*$P < 0.05$). (All the groups were treated at the same time; therefore, there is only one PBS group. For clarity, we arranged the graphs by VNP/VLP formulation.)

Figure 5.

Therapeutic effects of CPMV-1V209, CCMV-1V209, and Qβ-1V209 particles in the in vivo CT26 colon cancer model. (A) Timeline of CT26 cell inoculation and treatment. (B) Tumor growth curves. Blue arrows indicate the treatment days. (C) Volumetric scatter plot of individual tumors on day 22. Data are means ± SEM ($n = 5$). The results were compared by one-way ANOVA with Tukey's multiple comparisons test (**$P < 0.01$ and *$P < 0.05$). (D) Survival rates of tumor-bearing mice over 70 days (dashed line shows the intersection with median survival for each treatment). The results were compared using the log-rank
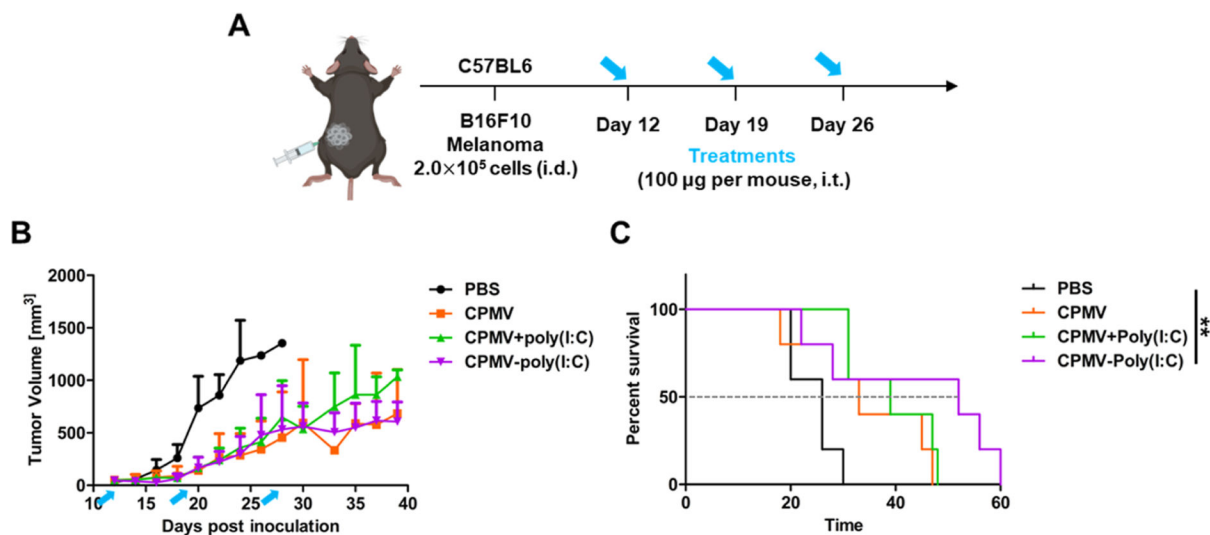
(Mantel–Cox) test (**P < 0.01 and *P < 0.05). (E) Relative body weight of tumor-bearing mice over 40 days.

Figure 6.
Therapeutic effect of CPMV-poly(I:C) particles in the in vivo B16F10 melanoma model. (A) Timeline of B16F10 cell inoculation and intratumoral particle injections. (B) Relative tumor volume in tumor-bearing mice following the injection of PBS, CPMV, CPMV + poly(I:C), or CPMV-poly(I:C). Blue arrows indicate the treatment days. Data are means ± SEM (n = 5). (C) Survival rates of tumor-bearing mice over 60 days (dashed line shows the intersection with median survival for each treatment). The results were compared using the log-rank (Mantel–Cox) test (**P < 0.01).